Mon. Not. R. Astron. Soc. **302,** 197–202 (1999)

The optical interstellar spectrum of κ Vel (HD 81188) and a measurement of interstellar cloud turbulence

S. K. Dunkin★ and I. A. Crawford

Department of Physics and Astronomy, University College London, Gower Street, London WC1E 6BT

Accepted 1998 September 9. Received 1998 August 11; in original form 1998 April 15

ABSTRACT

We present ultra-high resolution ($R \approx 10^6$) observations of lines due to interstellar Na I D, Ca II K, K I and Ti II towards κ Vel (HD 81188). Five velocity components are identified in both Na I and Ca II, and two in K I; an upper limit is recorded for Ti II. The very high spectral resolution has enabled us to resolve fully the intrinsic interstellar line profiles, and thereby obtain reliable measurements of the velocity dispersion parameters (b-values) for all identified velocity components. By comparing the observed b-values for Na I and K I, which differ in mass by almost a factor of 2, it has been possible to derive the kinetic temperature (T_k) and line-of-sight rms turbulent velocity (v_t) simultaneously for the two clouds identified in both elements. We obtain rigorous upper limits of 0.46 and 0.33 km s^{-1} for v_t in these two clouds, which are definitely subsonic at the measured temperatures. The three-dimensional turbulent velocity ($\equiv \sqrt{3} \times v_t$) is also almost certainly subsonic for both components, although it might just exceed the isothermal sound speed if the kinetic temperatures were close to the lower limits permitted by the line-profile analysis.

Key words: stars: individual: κVel – turbulence – ISM: atoms – ISM: clouds – ISM: structure.

1 INTRODUCTION

κ Vel (HD 81188) is a bright ($V = 2.5$), early-type (B2IV) southern star, having galactic coordinates $l = 275.^\circ88$, $b = -3.^\circ54$. It is probably a member of the nearby Scorpio-Centaurus OB association, which occupies most of the fourth galactic quadrant ($270^\circ \lesssim l \lesssim 360^\circ$; Blaauw 1964; de Geus, Lub & van de Grift 1990). The *Hipparcos* trigonometric distance of 165 ± 13 pc (ESA 1997) is significantly greater than the photometric distance of 102 pc estimated in earlier work (Crawford 1991), but is still consistent with Sco-Cen membership. The star is moderately reddened, with a colour excess of $E(B-V) = 0.11$, obtained from the Tycho B and V magnitudes (ESA 1997) and the intrinsic colours of Deutschman, Davis & Schild (1976).

To our knowledge, interstellar lines towards κ Vel were first reported by Buscombe & Kennedy (1962), who detected the interstellar Ca K line using hi-resolution photographic spectroscopy. More recently, Crawford (1991) obtained much higher resolution observations ($R = 83\,000$; 3.6 km s^{-1} FWHM) of the interstellar Ca II K and Na I D_2 lines as part of a study of the interstellar medium towards the Sco-Cen OB association. These revealed the presence of two Na I and Ca II velocity components (separated by 5 km s^{-1}), and it was clear that the strongest of these was intrinsically very narrow (the lines were not resolved, and b-value upper limits of 1.5 and 2.0 km s^{-1} were obtained for the Na I and Ca II lines respectively).

In an attempt to measure the intrinsic widths of these very narrow lines, and to determine if useful information about the physical state of the interstellar medium could be extracted from the resolved line profiles, we have now re-observed the star using the Ultra-High-Resolution Facility (UHRF) at the Anglo-Australian Telescope (see Diego et al. 1995 for a description of the instrument).

2 OBSERVATIONS

Observations of interstellar Na I D_1, Ca II K, K I and Ti II towards κ Vel were obtained with the UHRF in 1994 April and June. Table 1 lists the lines observed, and the dates and exposure times of the observations. The detector was a Tektronix CCD (1024×1024 24-μm pixels). The spectrograph was used in conjunction with an image slicer (Diego 1993), and the CCD output was binned by a factor of 8 in the spatial direction in order to reduce the readout noise associated with reading out the very broad spectrum which results. The velocity resolution, measured with the aid of a stabilized He-Ne laser, was determined to be 0.32 ± 0.01 km s^{-1} ($R = 940\,000$) for both dates.

The spectra were extracted using the FIGARO data-reduction package (Shortridge 1988) at the UCL Starlink node. Scattered light was measured from the interorder region and subtracted. Wavelength calibration was performed using a Th-Ar lamp. Once wavelength-calibrated, the spectra were converted to the heliocentric velocity frame (adopting the rest wavelengths given in

★ E-mail: skd@star.ucl.ac.uk

Table 1). Multiple exposures (Table 1) were co-added, and the resulting spectra were normalized by division of low-order polynomial fits to the continua on either side of the absorption lines. In the case of the Na I D_1 line, atmospheric water lines have been removed by division of an atmospheric template spectrum (as described by Barlow et al. 1995). The resulting spectra are shown in Fig. 1.

There is some evidence that that the background subtraction described above may have underestimated the true amount of scattered light in the system, and indeed it was found that an additional subtraction of 4 per cent of the continuum intensity resulted in a much better fit to the interstellar Na D_1 line profile. For the D_1 line we have subtracted this additional background, but have included the effect of a 4 per cent background error in the errors quoted on the equivalent widths and column densities (Table 2). Although we have no independent way of determining if the other lines are also affected by uncorrected scattered light, it seems quite likely that they are, and we have likewise allowed for a 4 per cent background error in the analysis. However, we note that this additional zero-level uncertainty makes a negligible difference to the intrinsic linewidths, which comprise the most important results of this paper.

Table 1. Observations towards κ Vel used in this work. Wavelengths and f-values are taken from Morton (1991).

Line	λ_0 (Å)	f	UT Date	Exp. time ($n \times$ sec)
Na I D_1	5895.924	3.18×10^{-1}	12-06-94	4×600
Ca II K	3933.663	6.35×10^{-1}	12-06-94	2×600
K I	7698.974	3.39×10^{-1}	24-04-94	2×600
Ti II	3383.768	3.40×10^{-1}	24-04-94	1×1200

3 RESULTS

Fig. 1 shows the observed spectra. The observed line profiles were modelled using the DIPSO data analysis program (Howarth, Murray & Mills 1993), and the best-fitting profiles are shown as smooth profiles superimposed on the observations. The resulting line profile parameters (heliocentric velocity, $v_{\rm helio}$, velocity dispersion, b, and column density, N) are listed in Table 2.

3.1 Na I D

Crawford (1991) identified two interstellar Na D velocity components towards κ Vel. However, the much higher resolution available with the UHRF has revealed the presence of at least five; both the $v_{\rm helio} = +8$ and $+13$ km s^{-1} components identified in the earlier work are here shown to consist of two, previously unresolved, components, while the high signal-to-noise ratio of the present data has also revealed an additional weak component at $v_{\rm helio} = +16.6$ km s^{-1}. The resolution of the UHRF is such that the 1.04 km s^{-1} hyperfine splitting of the sodium doublet is resolved (Fig. 1), which places very tight constraints on the range of parameters able to model the lines accurately.

In particular, we find that the strongest Na I absorption feature, at $v_{\rm helio} \approx 8.4$ km s^{-1}, is best fitted by two very narrow velocity components at $v_{\rm helio} = 8.25$ and 8.62 km s^{-1}, having b-values of 0.72 and 0.46 km s^{-1} respectively. It is true that these components are severely blended, which may give rise to some doubt as to their reality. In an attempt to demonstrate the existence of this velocity structure, we have computed several models for the strongest absorption component using a single cloud, and varying the b- and log N values to produce a fit to the data, and we found that no single cloud model could fit both the wings and the hyperfine structure in the core simultaneously. The best fit we could produce under the assumption of a single component ($v_{\rm helio} = 8.40$ km s^{-1}; $b = 0.69 \pm 0.04$ km s^{-1}; log $N = 11.94 \pm 0.02$ cm^{-2}) is shown in

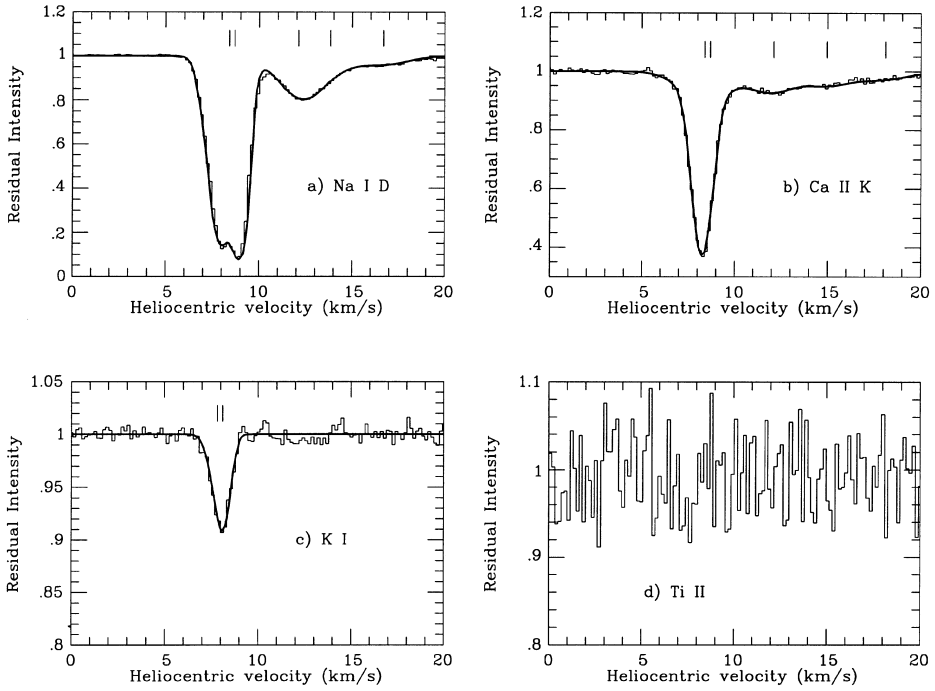

Figure 1. Theoretical line profiles (thick smooth lines) are shown plotted on observed spectra of (a) Na I D, (b) Ca II K and (c) K I. The Ti II spectrum (d) shows no evidence for the presence of an interstellar absorption line. The tickmarks indicate the positions of the theoretical cloud models listed in Table 2.

Table 2. Equivalent widths (w_λ) and line profile parameters derived for the lines of Na I D, K I, Ti II and Ca II K towards κ Vel. The errors on w_λ are 1σ values and include an assumed 4 per cent zero-level error (see Section 2).

Ion	w_λ (mÅ)	$v_{\rm helio}$ (km s^{-1})	$\Delta v_{\rm helio}$ (km s^{-1})	b (km s^{-1})	Δb (km s^{-1})	log$N$ (cm^{-2})	Δlog N (cm^{-2})
Na I D_1	57.7 ± 2.3	8.25	8.20–8.35	0.72	0.62–0.80	11.74	11.65–11.87
		8.62	8.55–8.69	0.46	0.40–0.50	11.58	11.43–11.73
		12.14	12.08–12.28	1.40	1.32–1.52	11.07	11.03–11.10
		13.80	13.50–14.20	1.40	1.17–1.65	10.45	10.30–11.55
		16.60	16.35–16.85	1.75	1.50–1.95	10.45	10.40–11.55
Ca II K	19.5 ± 0.8	8.25	8.20–8.34	0.68	0.60–0.78	11.21	11.18–11.27
		8.40	8.24–8.55	1.80	1.40–2.05	10.70	10.62–10.80
		11.90	11.78–12.08	1.60	1.30–1.75	10.48	10.45–10.53
		14.90	14.70–15.35	1.90	1.70–2.10	10.40	10.35–10.46
		18.00	17.50–18.40	1.80	1.40–2.10	10.10	10.05–10.20
K I	2.75 ± 0.14	7.85	7.75–7.96	0.60	0.52–0.66	10.00	9.96–10.06
		8.22	8.14–8.30	0.42	0.33–0.48	9.75	9.71–9.82
Ti II	≤0.46	—	—	—	—	≤9.41	—

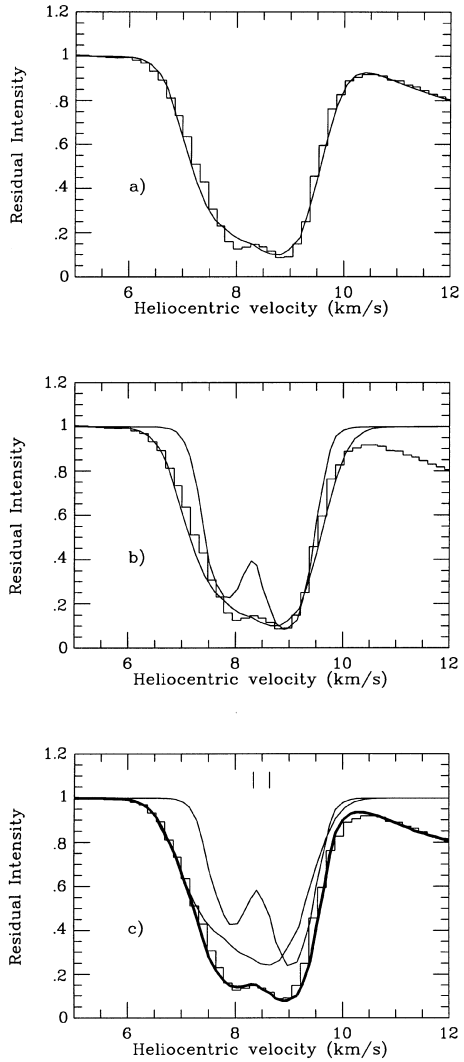

Figure 2. (a) The best-fitting single cloud fit to the observed profile of the strongest absorption line; note that this model does not reproduce the hyperfine structure in the core of the line. (b) Narrow and broad single-cloud models. (c) Our preferred final model (thick line) and its individual components; see text for details.

Fig. 2(a), and although a good fit is made to the wings of the line, the model is unable to reproduce the hyperfine structure seen in the core. Fig. 2(b) shows two single-cloud models superimposed, one narrow ($b = 0.46$ km s^{-1}), one broad ($b = 0.72$ km s^{-1}). These are the b-values of the individual components of the two-cloud model; it is clear that neither fits the observed line well, and we are forced to conclude that the observed profile is a blend of contributions from more than one cloud. Fig. 2(c) shows our preferred two-component fit on the same scale.

The presence of strong interstellar Na D lines towards κ Vel appeared anomalous, given the photometric distance of 102 pc estimated by Crawford (1991), as this would have placed the star well in the foreground of the dense clouds (distances ≈170–200 pc; Dame et al. 1987) which dominate interstellar absorption in the fourth galactic quadrant (cf. fig. 7 of Dame et al. 1987, and also fig. 1a of Crawford 1991). The new *Hipparcos* distance of 165 ± 13 pc has largely eliminated this anomaly. It now seems most likely that, like other strong interstellar lines observed in this galactic longitude range, these components arise in outlying gas associated with the well-defined 'ridge' of giant molecular clouds identified by Dame et al. (1987; cf. also the discussion by Crawford 1992). The low radial velocities of these components relative to the local standard of rest ($v_{\rm LSR} = v_{\rm helio} - 14.6$ km s^{-1} towards κ Vel) are consistent with this interpretation.

3.2 Ca II K

A total of five interstellar absorption components were detected towards κ Vel in the Ca II K line, and Table 2 lists the derived line profile parameters for each component. We found that the strongest Ca K component at $v_{\rm helio} \approx 8.3$ km s^{-1}, which appeared single in Crawford's (1991) lower resolution spectra, could not be modelled accurately with a single cloud, and required two components, of different b-values, to fit simultaneously the wings and the core of the line. The presence of two components needed to fit the Ca K line is fully consistent with the two Na components at very similar velocities (Table 2). It is true that one of these Ca components has a significantly larger b-value than its Na counterpart, but this is often found to be the case with interstellar Ca lines (and is generally attributed to the Ca ions lying primarily in the warmer/more turbulent outer regions of diffuse interstellar clouds; e.g. Barlow

et al. 1995).

The remaining three Ca II components are all much weaker, and lie at more redshifted velocities (Fig. 1b). We note that κ Vel has a strong stellar Ca K line (of variable velocity, as the star is a spectroscopic binary), which raises difficulties in defining the local continuum for these weak absorption components. Nevertheless, we are fairly confident in the reality of these redshifted components because (i) they occupy the same velocity range as the weak Na I components (extending to $v_{\rm helio} \approx +20$ km s^{-1}), and (ii) the total Ca K equivalent width with these features included (19.5 ± 0.8 mÅ) agrees well with the value of 22 ± 3 mÅ obtained at lower resolution by Crawford (1991).

3.3 K I

The interstellar K I line towards κ Vel is much weaker than either the Na or Ca lines, but nevertheless a good signal-to-noise spectrum was obtained (Fig. 1c). As is the case for the Na D lines, the K I resonance line is split by hyperfine structure. This structure has not been resolved here (it amounts to only 0.35 km s^{-1}; e.g. Welty, Hobbs & Kulkarni 1994), but it does broaden the line profile and has been included in the analysis.

It was found that, while a single cloud model ($v_{\rm helio} = +8.0$ km s^{-1}; $b = 0.63 \pm 0.13$ km s^{-1}; $\log N = 10.22 \pm 0.08$ cm^{-2}) was able to fit the K I line fairly well, the two-cloud model listed in Table 2 gave a somewhat better fit, especially in the wings of the profile. A two-cloud model is also favoured because of the two-cloud model required to fit the Na D_1 and Ca K lines. As Na I and K I have similar ionization potentials (5.1 and 4.3 eV respectively) and similar grain-surface adsorption binding energies (Barlow 1978), we expect both species to coexist spatially within diffuse interstellar clouds. Following this reasoning, the two K I components were given a velocity separation (0.37 km s^{-1}) equal to that of the two Na I components, and it is clear (Fig. 1c) that this assumption is fully consistent with the observed line profile. We consider that the small (0.4 km s^{-1}) absolute velocity difference between Na I and K I components listed in Table 2 probably results from wavelength calibration uncertainties.

We note that, as for the Na I components, the b-values for the K I lines are very narrow, 0.42 and 0.60 km s^{-1} for the 8.22 and 7.85 km s^{-1} components respectively. These are very similar to, though slightly smaller than, the Na I values (Table 2), and follow the same trend in the sense that the more blueshifted component is the broader of the two. Of course, this is what we would expect if Na I and K I coexist spatially within the clouds.

3.4 Ti II

The spectral region of the Ti II line at 3384 Å shows no obvious absorption due to this ion (Fig. 1d). We note that Welsh et al. (1997) have carried out a survey of interstellar Ti II toward 42 southern hemisphere stars, two of which (o Vel and ϕ Vel) are within a few degrees on the sky of κ Vel. Welsh et al. derived only an upper limit of w_λ(Ti II) < 2.3 mÅ towards o Vel ($l = 270°$, $b = -6.8°$, $d = 152$ pc; ESA 1997), which is consistent with the non-detection of of Ti II towards κ Vel.

4 DISCUSSION

The main advantage conferred on interstellar studies by the UHRF is its ability to resolve the profiles of narrow interstellar absorption lines, and, as a consequence, to place well-defined limits on the intrinsic velocity dispersions (b-values). The b-value is related to the thermal and 'turbulent' broadening of the line profile through the expression

$$b = \sqrt{\frac{2kT_{\rm k}}{m} + 2v_{\rm t}^2}, \qquad (1)$$

where $T_{\rm k}$ is the kinetic temperature of the cloud, $v_{\rm t}$ is the line-of-sight rms turbulent velocity, m is the mass of the element under consideration, and k is Boltzmann's constant. In principle, by solving equation (1) for atoms having a wide range of masses, it is possible to obtain $T_{\rm k}$ and $v_{\rm t}$ simultaneously. In practice, this will be possible only if the b-values are well-constrained (through high-resolution/high-signal-to-noise spectroscopy), and for species which coexist spatially within the cloud.

Here we have suitable measurements for Na I D_1 and K I. These elements differ by almost a factor of 2 in mass (23 and 39 amu respectively) and, as discussed in Section 3.3, are thought to occur predominantly in the same regions of the clouds. As a result, we have been able to solve equation (1) for the observed Na I and K I b-values for both clouds. Under the conservative (but probably incorrect) assumption that the main absorption feature for both atoms consists of only one velocity component, we obtain $T_{\rm k} = 266$ K and $v_{\rm t} = 0.38$ km s^{-1}. For our preferred line profile fits containing two velocity components (Table 2), we obtain $T_{\rm k} = 532$ K, $v_{\rm t} = 0.26$ km s^{-1} for the first cloud [v(Na) = 8.25 km s^{-1}], and $T_{\rm k} = 118$ K, $v_{\rm t} = 0.25$ km s^{-1} for the second cloud [v(Na) = 8.62 km s^{-1}].

Of course, there are observational uncertainties on the measured b-values (Table 2), which must be allowed for in the determination of the possible range of values of $T_{\rm k}$ and $v_{\rm t}$. In order to do this, we have determined the values of $T_{\rm k}$ and $v_{\rm t}$ which are consistent with b-values in the observed range (where we have performed the calculation for a grid of b-values, 0.01 km s^{-1} apart, between the minimum and maximum values permitted by the observations). An example of this analysis is shown in Table 3. Table 4 summarizes the final results, and it is interesting to note that the ranges of temperatures and turbulences obtained are actually not very different under the assumptions of one (conservative) or two (preferred) velocity components. Note also that, for the two component case, the best-fitting line-of-sight rms turbulence is almost identical in both clouds ($v_{\rm t} \approx 0.25$ km s^{-1}), despite the fact that one of them appears to be significantly hotter than the other.

There has long been a debate over whether internal motions in diffuse interstellar clouds are subsonic or supersonic (e.g. Welty et al. 1994, and references therein). It is generally assumed that diffuse cloud turbulence must be subsonic, owing to the lack of obvious energy sources needed to maintain highly dissipative supersonic turbulence, but direct measurements have been rare because of the very high spectral resolution required. For example, Blades, Wynne-Jones & Wayte (1980), Hobbs & Welty (1991) and Welty et al. (1994), using resolving powers of $R \approx 6 \times 10^5$, have demonstrated subsonic turbulence for interstellar clouds towards a number of stars, but only by *assuming* an average kinetic temperature of 80 K (obtained from the rotational excitation of H_2; Spitzer 1978, p. 51).

The isothermal sound speed, $C_{\rm s}$, is given (e.g. Spitzer 1978, pp. 216–7) by

$$C_{\rm s} = \sqrt{\frac{kT_{\rm k}}{\mu}}, \qquad (2)$$

Table 3. Kinetic temperatures and line-of-sight rms turbulences calculated from equation (1) for the 8.62 km s^{-1} cloud in Na. The top number for each calculation is the temperature (K), and the lower number the turbulence (km s^{-1}). Calculations have been made for the entire range of allowable *b*-values (Table 2), and therefore encompass all possible temperature and turbulence values for this cloud. A similar table can also be made for the 8.25 km s^{-1} cloud; a summary for both clouds may be found in Table 4.

		Na D_1										
	b (km s^{-1})	0.40	0.41	0.42	0.43	0.44	0.45	0.46	0.47	0.48	0.49	0.50
	0.33	172	199	226	255							
		0.13	0.11	0.08	0.02							
	0.34	149	176	204	232	261						
		0.16	0.14	0.12	0.09	0.05						
	0.35	126	153	181	209	239	261					
		0.19	0.17	0.15	0.13	0.10	0.06					
	0.36	102	129	157	186	215	245	275				
		0.21	0.19	0.18	0.16	0.14	0.11	0.08				
	0.37	78	105	133	161	190	220	251	282	314		
		0.23	0.21	0.20	0.18	0.17	0.15	0.12	0.09	0.04		
	0.38	52	80	107	136	165	195	226	257	289	321	
		0.25	0.24	0.22	0.21	0.19	0.17	0.16	0.13	0.10	0.06	
	0.39	27	54	82	110	139	169	200	231	263	295	329
K I		0.27	0.25	0.24	0.23	0.22	0.20	0.18	0.16	0.14	0.12	0.08
	0.40		27	55	84	113	143	173	204	236	269	302
			0.27	0.26	0.25	0.24	0.22	0.21	0.19	0.17	0.15	0.13
	0.41			28	56	86	115	146	177	209	242	275
				0.28	0.27	0.26	0.24	0.23	0.22	0.20	0.18	0.16
	0.42				29	58	88	118	149	181	214	247
					0.29	0.28	0.26	0.25	0.24	0.22	0.21	0.19
	0.43					29	59	90	121	153	185	219
						0.29	0.28	0.27	0.26	0.24	0.23	0.21
	0.44						30	60	92	124	156	189
							0.30	0.29	0.28	0.27	0.25	0.24
	0.45							31	62	94	126	159
								0.31	0.30	0.29	0.27	0.26
	0.46								31	63	96	129
									0.31	0.30	0.29	0.25
	0.47									32	64	98
										0.32	0.31	0.30
	0.48										33	66
											0.33	0.32

Table 4. Summary of the kinetic temperatures and turbulences derived for the κ Vel sightline under the assumption of (a) one velocity component and (b) two velocity components (see text for details).

Components	$v_{\rm helio}$ (km s^{-1})	$T_{\rm k}$ (K)	$v_{\rm t}$ (km s^{-1})	$C_{\rm s}$ (km s^{-1})	$\Delta T_{\rm k}$ (K)	$\Delta v_{\rm t}$ (km s^{-1})	$\Delta C_{\rm s}$ (km s^{-1})
(a) One-component fit:	8.40	266	0.38	1.32	43–749	0.51–0.03	0.53–2.21
(b) Two-component fit:	8.25	532	0.26	1.86	41–858	0.46–0.02	0.52–2.36
	8.62	118	0.25	0.88	27–329	0.33–0.02	0.42–1.46

where μ is the mean mass per particle ($1.27m_{\rm H}$ for an atomic hydrogen gas containing 10 per cent He by number).

Table 4 lists $C_{\rm s}$ for the best-fitting kinetic temperatures, and also the range in $C_{\rm s}$ for the range of temperatures permitted by observation. It can be seen that, even allowing for the fact that a low $T_{\rm k}$ implies both a high $v_{\rm t}$ and a low $C_{\rm s}$, in all cases $v_{\rm t} < C_{\rm s}$, so the one-dimensional turbulent velocity is definitely subsonic for an H I gas. It is true that, if a significant amount of H was in the form of H_2, μ would be higher and $C_{\rm s}$ smaller. However, there is no evidence for significant molecular gas towards κ Vel, and even if half the hydrogen nuclei were locked up in H_2 the isothermal sound speed would be reduced by only approximately 14 per cent, leaving the basic conclusion unchanged.

Strictly speaking, we should compare the *three-dimensional* turbulent velocity ($\equiv\sqrt{3}\times v_{\rm t}$) with $C_{\rm s}$ in order to conclusively demonstrate subsonic turbulence (e.g. Hobbs & Welty 1991). In this case we see that, while our preferred values of $T_{\rm k}$ and $v_{\rm t}$ still imply subsonic turbulence, it is possible for the three-dimensional turbulent velocity to be supersonic for kinetic temperatures near the lower end of the ranges listed in Table 4. Specifically, an additional search of the ($T_{\rm k}$, $\sqrt{3}v_{\rm t}$) parameter space revealed that the latter quantity exceeds $C_{\rm s}$ only if $T_{\rm k} \lesssim 90$ K for the 8.25 km s^{-1} component, and $\lesssim$33 K for the 8.62 km s^{-1} component. Thus, although we cannot absolutely rule out the

possibility that the three-dimensional turbulent velocity exceeds the local sound speed, we can show that this is only possible if the kinetic temperatures are very close to the lower limits listed in Table 4.

5 CONCLUSIONS

We have obtained ultra-high resolution ($R \approx 10^6$) observations of interstellar Na I D, Ca II K, K I and Ti II towards κ Vel (HD 81188). We have identified five discrete velocity components in Na I, five in Ca II, and two in K I; Ti II was not detected. We have derived well-constrained line profile parameters for all the identified velocity components.

By comparing the *b*-values obtained for Na I and K I we have been able to obtain both the kinetic temperature, and the line-of-sight rms turbulent velocity, for the two strongest velocity components present towards this star. In both cases the line-of-sight turbulent velocity ($v_t \approx 0.25$ km s^{-1}) is definitely subsonic at the measured temperatures. The three-dimensional turbulent velocity ($\equiv \sqrt{3} \times v_t$) is also almost certainly subsonic for both components, although formally this quantity might just exceed the isothermal sound speed if the kinetic temperatures were very close to the lower limits permitted by the line-profile analysis.

ACKNOWLEDGMENTS

We thank PPARC for financial support, and PATT for the allocation of telescope time. We also thank M. J. Barlow, and an anonymous referee, for helpful comments on the original manuscript.

REFERENCES

Barlow M. J., 1978, MNRAS, 183, 417
Barlow M. J., Crawford I. A., Diego F., Dryburgh M., Fish A. C., Howarth I. D., Spyromilio J., Walker D. D., 1995, MNRAS, 272, 333
Blaauw A., 1964, ARA&A, 2, 213
Blades J. C., Wynne-Jones I., Wayte R. C., 1980, MNRAS, 193, 849
Buscombe W., Kennedy P. M., 1962, MNRAS, 124, 195
Crawford I. A., 1991, A&A, 247, 183
Crawford I. A., 1992, MNRAS, 254, 264
Dame T. M., et al., 1987, ApJ, 322, 706
de Geus E. J., Lub J., van de Grift E., 1990, A&AS, 85, 915
Deutschman W. A., Davis R. J., Schild R. E., 1976, ApJS, 30, 97
Diego F., 1993, Appl. Opt., 32, 6284
Diego F. et al., 1995, MNRAS, 272, 323
ESA, 1997, The *Hipparcos* and Tycho Catalogues, ESA SP-1200
Hobbs L. M., Welty D. E., 1991, ApJ, 368, 426
Howarth I. D., Murray J., Mills D., 1993, Starlink User Note No. 50
Morton D. C., 1991, ApJS, 77, 119
Shortridge K., 1988, Starlink User Note No. 86
Spitzer L., 1978, Physical Processes in the Interstellar Medium. John Wiley, New York
Welsh B. Y., Sassen T., Craig N., Jelinsky S., Albert C. E., 1997, ApJS, 112, 507
Welty D. E., Hobbs L. M., Kulkarni V. P., 1994, ApJ, 436, 152

This paper has been typeset from a TEX/LATEX file prepared by the author.